THE JOURNAL OF PHYSICAL CHEMISTRY Letters

Letter

pubs.acs.org/JPCL

Understanding the Thickness-Dependent Performance of Organic Bulk Heterojunction Solar Cells: The Influence of Mobility, Lifetime, and Space Charge

Thomas Kirchartz,*[,†] Tiziano Agostinelli,[†] Mariano Campoy-Quiles,[‡] Wei Gong,[†,§] and Jenny Nelson[†]

[†]Department of Physics and Centre for Plastic Electronics, Imperial College London, South Kensington Campus, London SW7 2AZ, United Kingdom

[‡]Institut de Ciència de Materials de Barcelona, UAB Campus, 08193 Bellaterra, Spain

[§]Key Laboratory of Luminescence and Optical Information, Ministry of Education and Institute of Optoelectronics Technology, Beijing Jiaotong University, Beijing 100044, People's Republic of China

Supporting Information

ABSTRACT: We investigate the reasons for the dependence of photovoltaic performance on the absorber thickness of organic solar cells using experiments and drift-diffusion simulations. The main trend in photocurrent and fill factor versus thickness is determined by mobility and lifetime of the charge carriers. In addition, space charge becomes more and more important the thicker the device is because it creates field free regions with low collection efficiency. The two main sources of space-charge effects are doping and asymmetric mobilities. We show that for our experimental results on Si-PCPDTBT:$PC_{71}BM$ (poly[(4,40-bis(2-ethylhexyl)dithieno[3,2-*b*:20,30-*d*]silole)-2,6-diyl-*alt*-(4,7-bis(2-thienyl)-2,1,3-benzothiadiazole)-5,50-diyl]:[6,6]-phenyl C71-butyric acid methyl ester) solar cells, the influence of doping is most likely the dominant influence on the space charge and has an important effect on the thickness dependence of performance.

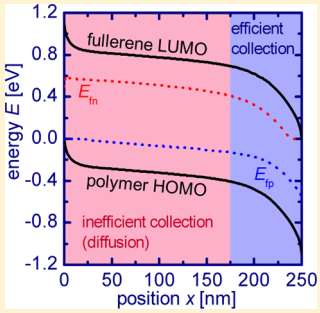

SECTION: Energy Conversion and Storage; Energy and Charge Transport

One of the main design challenges for thin-film solar cells is to find the ideal absorber thickness that represents the best compromise between strong light absorption and efficient charge carrier collection. Finding such a compromise between absorption and collection is particularly challenging in organic thin-film solar cells. Because of the low mobility-lifetime products[1−3] of organic solar cells, the optimum absorber thicknesses are often limited to ∼100 nm and less. Larger absorber thicknesses lead to increased collection losses of charge carriers due to nongeminate recombination[4] that overcompensate the gain in absorptance in most cases. Because of the smooth interfaces and low thicknesses, organic solar cells are strongly affected by interference effects, which complicate device optimization further. The percentage of light absorbed by polymer:fullerene solar cells consisting of thin and smooth layers is not monotonously increasing[5] but features different maxima caused by the interferences of standing waves in the layer stack. The combination of insufficient charge carrier collection and interference effects dictates that the vast majority of polymer:fullerene solar cells will have the best device efficiency close to the first interference maxima (typically at just below 100 nm absorber layer thickness).[4] Only poly(3-hexylthiophene) (P3HT):PCBM[6−9] and a small number of other high mobility polymers blended with PCBM[4,10] are able to make use of the increased absorption at the second interference maximum (typically around 200−250 nm). All other polymers waste 20−40%[6,11−15] of the total photon flux due to their insufficient electronic properties.

To overcome this limitation, a good physical understanding of the factors controlling the thickness dependent performance of polymer:fullerene solar cells is crucial. With many well-studied, highly efficient polymer:fullerene solar cells showing little sign of field-dependent geminate recombination,[16−19] the main loss mechanism at larger thicknesses is nongeminate recombination of already separated charge carriers. In the literature, the charge-carrier collection process is often assumed to be described by carriers drifting in the built-in electric field to the contact. The characteristic quantity describing this process is the ratio of drift length $L_{dr} = \mu\tau F$ and device thickness d.[1,20] Here μ is the mobility of the charge carriers, τ is the lifetime, and F is the electric field. The concept of a drift length is a useful starting point because it explains why charge carrier collection is voltage- and thickness-dependent. When the space charge in the device is negligible, the electric field is $F = (V_{bi} - V)/d$, where V_{bi} is the built-in voltage, and thus

$$\frac{L_{dr}}{d} = \mu\tau\frac{V_{bi} - V}{d^2} \quad (1)$$

Received: October 11, 2012
Accepted: November 12, 2012
Published: November 12, 2012

That means that collection scales with $1/d^2$, and it is voltage-dependent.[20] At short circuit, the field is much higher than at the maximum power point, so the short circuit current density J_{sc} might still be high in thick cells, whereas the fill factor *FF* will deteriorate much faster with smaller mobilities μ, smaller lifetimes τ, or larger thicknesses d.

Whereas the concept of drift lengths gives a qualitative interpretation for reduced *FF*s and photocurrents at larger thicknesses, it is, in general, not sufficient for a quantitative interpretation. First, the concept of a mobility-lifetime product assumes that it does not depend on voltage. However, it has been shown that the mobility increases and the lifetime decreases with carrier concentration, leading to an expected slight decrease of the $\mu\tau$-product with carrier concentration (see Supporting Information, section 8), voltage, and light intensity.[2] Second, the concept of a drift length is based on the assumption of a constant electric field, which is a decent approximation in thin devices (<100 nm) at short circuit or reverse bias. At larger thicknesses and in forward bias, the approximation of constant electric fields gets worse due to the strong influence of the space charge of the injected charges in organic materials with their low dielectric constants. The electric field can further be altered by charged defects, that is, by doping,[21,22] and by photogenerated charges that have different mobilities for electrons and holes.[23,24] Such asymmetric transport properties lead to a buildup of charge and change the electric field profile such that the collection of both charge carriers is equally efficient in the steady state and the whole device stays charge neutral.

We will investigate the reasons for the observed dependence of photovoltaic performance on the absorber layer thickness in a series of Si-PCPDTBT:$PC_{71}BM$[25,26] with layer thicknesses in the range between 119 and 352 nm. To understand the effect of space charge on the thickness-dependent current/voltage curves, we discuss the two cases of asymmetric mobilities[14,27,28] and doping[21,29−34] in comparison with an intrinsic, symmetric mobility case and an analytical approximation based on a spatially constant electric field. We suggest that in this particular case, the presence of fixed charge, that is, doping, describes the thickness-dependent behavior of the devices best and we confirm the presence of a doping concentration of roughly $N_A \approx 2 \times 10^{16}$ cm^{-3} using capacitance/voltage measurements (see Supporting Information Figures S1 and S2).[31,35] Note that the origin of the unintentional doping in organic semiconductors is, in general, not known,[36] although in the more extensively studied polythiophenes often oxygen and moisture are suggested as possible origins.[33,37,38] The doping type cannot be determined by capacitance measurements but can be identified as p-type doping from the thickness dependence of the short-circuit current density, as shown later.

Figure 1a shows the current voltage (*JV*) curves of four representative thicknesses that were measured. Each line corresponds to the average over all six cells on one substrate that was prepared with one spin speed. We then simulated the current/voltage curves at the same thicknesses with a combined optical and electrical model using the experimental data (light and dark *JV* curves) at 219 nm active layer thickness to adjust the parameters for the electrical multiple-trapping model (see Table 1 and Supporting Information for electrical parameters). The electrical model is described in more detail in ref 39 and is based on numerically solving the Poisson equation

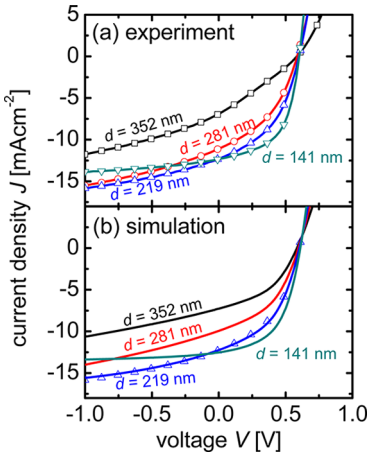

Figure 1. (a) Measured and (b) simulated *J*/*V* curves of SiPCPDTBT:$PC_{71}BM$ devices with four different thicknesses. The simulation is based on a fit of the electrical parameters to the cell with 219 nm active layer thickness (open triangles in panel b), and it takes the measured doping concentration into account. The parameters are given in Table 1 in the Supporting Information.

Table 1. Parameters That Change between Simulations[a]

name	symbol	p-type	asymmetric mobilities	intrinsic
electron mobility	μ_n [$cm^2/(V\,s)$]	10.9×10^{-4}	54.5×10^{-4}	10.9×10^{-4}
hole mobility	μ_p [$cm^2/(V\,s)$]	10.9×10^{-4}	2.2×10^{-4}	10.9×10^{-4}
p-type doping density	N_A [cm^{-3}]	2×10^{16}	0	0

[a]All other parameters are defined in Table 1 of the Supporting Information. Note that the mobilities given are band mobilities and apply only to the untrapped fraction of the charge carrier population.

$$\Delta\varphi = -\frac{\rho}{\varepsilon} \tag{2}$$

defining the relation between electrical potential φ, space charge density ρ, and permittivity ε and the continuity equations for electrons and holes. Recombination is assumed to be dominated by recombination between free carriers and between carriers occupying an exponential distribution of traps. The existence of traps is necessary to be able to reproduce the experimental ideality factor of the dark *JV* curve. Doping is introduced by adding a fixed and spatially independent charge to the space-charge density ρ via $\rho = q(p_{tot} - n_{tot} - N_A)$, where p_{tot} and n_{tot} are the total (free + trapped) hole and electron densities, N_A is the acceptor concentration and q is the elementary charge. The space-charge density ρ is then used to calculate the electric potential in the device using Poisson's equation (eq 2). Charge generation is assumed to be field-independent based on transient absorption measurements on the same material that show no change in charge generation yield as a function of electric field.[18] Note that we assume all parameters to be spatially independent and neglect all possible influences of a vertical composition grading (see Supporting Information, sections 10 and 11).

The optical model requires knowing the complex refractive index of the active layer, which was measured with spectroscopic ellipsometry (see Supporting Information) while the complex refractive indices of the contact layers

dx.doi.org/10.1021/jz301639y | J. Phys. Chem. Lett. 2012, 3, 3470−3475

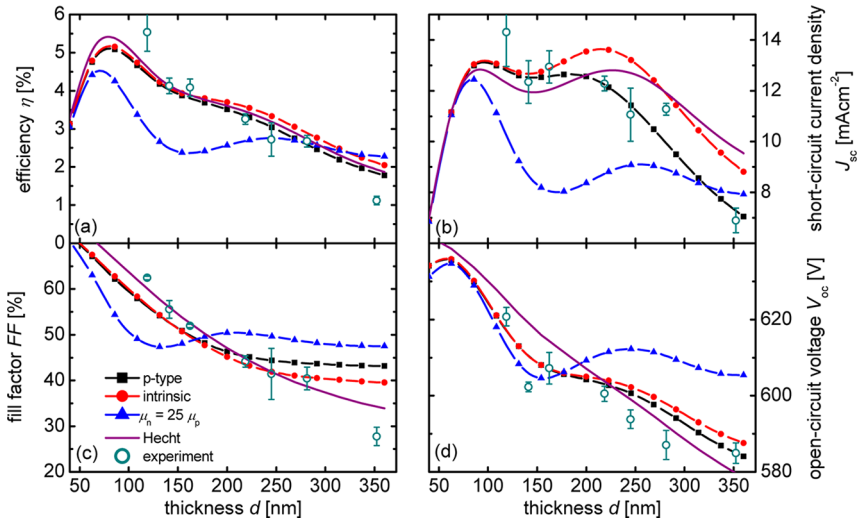

Figure 2. Thickness dependence of (a) efficiency, (b) short-circuit current density, (c) fill factor, and (d) open-circuit voltage for the experiment (symbols), three different simulations (with p-type doping and symmetric mobilities: line + square; without doping and with symmetric mobilities: line + circle; without doping and with asymmetric mobilities: line + triangle), and one analytical approximation (Hecht equation). The most dramatic impact of asymmetric conductivity caused by either doping or mobility asymmetries is the reduced short-circuit current at higher thicknesses that causes the efficiency to drop relative to the symmetric case.

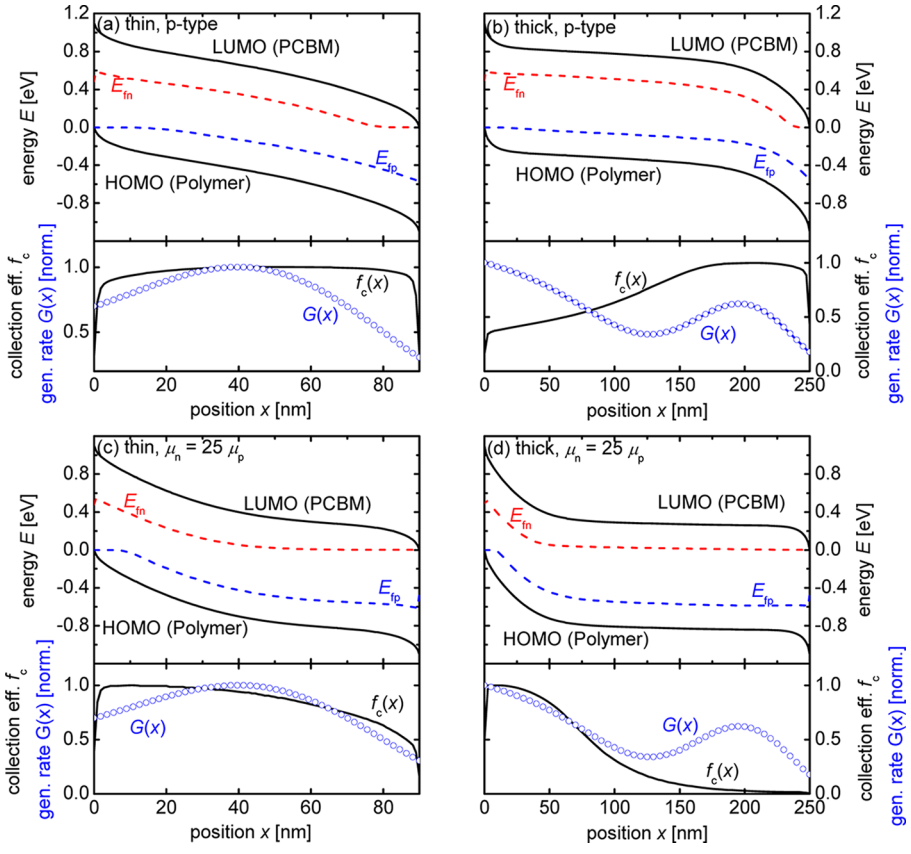

Figure 3. (a–d) Band diagrams of (a,c) a 90 nm thin solar cell with (a) p-type doping or (c) asymmetric mobilities at short circuit and one sun illumination compared with the analogous band diagrams of (b,d) a 250 nm thick solar cell. The collection efficiency plots show that in the thick cells the collection efficiency is only high in the depletion region, which means that the thick cells with doping or mobility asymmetry have a drastically reduced collection either close to the back contact (p-type doping) or close to the front contact ($\mu_n \gg \mu_p$).

were taken from refs 40–42. The position-dependent generation rate was then calculated using a matrix transfer algorithm as shown for instance in refs 43 and 44. The resulting simulations for the same four thicknesses are displayed in Figure 1b with the experimental data at 219 nm that were used for the calibration being indicated by open triangles. We assume that all parameters in the simulation are independent of cell thickness (see Table 1 in the Supporting Information) and use a p-type doping concentration ($N_A = 2 \times 10^{16}$ cm^{-3}) that is consistent with the Mott–Schottky analysis. Although the

dx.doi.org/10.1021/jz301639y | J. Phys. Chem. Lett. 2012, 3, 3470–3475

general qualitative trend in device performance is reproduced by the simulation, there are quantitative differences between simulation and experiment, suggesting that not all electrical parameters are thickness-independent.

Figure 2 shows the four parameters, efficiency η, short-circuit current density J_{sc}, fill factor *FF*, and open circuit voltage V_{oc} as a function of device thickness comparing three different numerical models and one analytical equation with the experimental results. The models are (i) with p-type doping as used for Figure 1a, (ii) intrinsic, and (iii) intrinsic but with a large mobility asymmetry, assuming that the electron mobility μ_n is much larger than the hole mobility μ_p. The analytical model is the so-called Hecht[45] equation for the photocurrent[20]

$$J_{ph} = -2q\bar{G}\mu\tau\frac{V_{bi} - V}{d}\left(1 - \exp\left(\frac{-d^2}{2\mu\tau(V_{bi} - V)}\right)\right) \quad (3)$$

based on the assumption of constant electric fields and with the mobility-lifetime product $\mu\tau$ and the built-in voltage V_{bi} as the free parameters. Here we assume that electrons and holes have the same mobility, that is, that there is only one $\mu\tau$ product, and fit the above equation to the photocurrent of the device at 219 nm thickness, obtaining $\mu\tau = 6.3 \times 10^{-10}$ cm^2/V and $V_{bi} = 0.65$ V. The optical generation as input for eq 3 is still calculated numerically, as done for the drift-diffusion simulations, but only the spatially averaged generation rate $\bar{G}$ is used. To obtain the current density under illumination, we add the experimental dark current (averaged over all pixels from the substrate with 219 nm thickness) to the photocurrent J_{ph}.

From the simulations, we can see that Si-PCPDTBT:PCBM has two interference maxima at around 90 and 250 nm, but the efficiency clearly peaks at the first interference maximum. The drop in efficiency is mainly caused by a drop in *FF*, which cannot be compensated by the increased absorption. The open-circuit voltage V_{oc} also decreases with thickness because the recombination at a given voltage increases linearly with thickness and the generation sublinearly. Therefore recombination and generation balance out at a lower V_{oc} for thicker devices.

The main difference between the different models is the behavior of J_{sc} as a function of thickness. In all cases, the two interference maxima are visible that are due to the optical generation rate that is the same for all models. However, the models with asymmetries in space charge (p-type doping, asymmetric mobilities) will modulate the electric field in the device, which will lead to a spatial variation of the charge collection efficiency. Therefore, these models will predict a drop of J_{sc} at lower thicknesses than the intrinsic model and the analytical model based on eq 3. The simulation with p-type doping predicts the trend in J_{sc} best. In particular, the trend is better than the case with n-type doping of the same magnitude, which is shown in Figure S8 in the Supporting Information.

To understand the thickness dependence of the device efficiency in the presence of space charge, we studied the simulated band diagrams (in short circuit under one sun illumination) shown in Figure 3 for thicknesses around the first (90 nm) and second interference maximum (250 nm) in the case of (a,b) p-type doping and (c,d) asymmetric mobilities. The first observation is the different influence of space charge on the band diagram depending on the active layer thickness. This is understood from the equation for the width

$$w = \sqrt{\frac{2\varepsilon(V_{bi} - V)}{qN_A}} \quad (4)$$

of the space-charge region as a function of the doping concentration N_A and the dielectric constant ε. Here q is the elementary charge. For a doping density $N_A = 2 \times 10^{16}$ cm^{-3}, a permittivity $\varepsilon = 3.8\varepsilon_0$, and an effective built-in voltage of $V_{bi} - V = 1$ V, we obtain a width $w = 145$ nm. Thus, at a thickness of $d = 90$ nm and the above parameters, the whole active layer is depleted with or without doping around short circuit. However, at $d = 250$ nm, the device is split into a part of the active region that is depleted and where the electric field is high and a part that is neutral and nearly field-free. In case of p-type doping, the space-charge region is close to the cathode, that is, not at the side from which the device is illuminated in our experiments. Thus, all electrons that are photogenerated in the field-free region close to the anode in Figure 3b will have to diffuse to the depletion zone at the cathode before the electric field will assist with extraction. Because of the large concentration of holes in the field-free region, this diffusion process will lead to a loss in electrons and finally to a loss of photocurrent. However, because the diffusion process is independent of electric field, the loss will be roughly the same at short circuit as compared with the maximum power point. This explains the substantial decrease in J_{sc} in doped cells seen in Figure 2b but also the higher *FF* relative to the intrinsic case in Figure 2c, which is due to the reduced voltage dependence of collection.

We define the collection efficiency f_c of charge carriers as the probability that a photon absorbed at a position x in the device will generate an electron and a hole that will both be collected at short circuit. The results for the calculation of the collection efficiency for the four cases are presented together with the corresponding generation rates in the lower frames of Figure 3a–d. From these results, we see that collection in the two thin cells is rather constant as a function of position; the collection efficiency of the thick doped cell is high only toward the cathode, that is, in the depletion region, where the electric field assists in separating the charge carriers.

In the case of the mobility asymmetry, the general behavior is the same as that for doping, with the only difference that the space-charge region in the thick cell (cf. Figure 3d) now forms at the contact that injects and extracts the slower carrier, that is, the anode in our example. The behavior of asymmetric mobilities with $\mu_n \gg \mu_p$ is therefore very similar to n-type doping, which would also create a space-charge region close to the anode and a field-free region toward the cathode. This implies that the collection efficiency in Figure 3d (solid line) is high close to the anode and low close to the cathode. In most cases, this situation is more beneficial for device performance because it creates the space-charge region on the illuminated side and improves collection where absorption is usually higher. The nonmonotonous behavior of the efficiency seen in Figure 2a is due to the fact that interferences shift the peak of the absorption such that it is not necessarily close to the front contact.

In conclusion, we have shown that doping as well as asymmetric mobilities affect the electric field and the collection efficiency in sufficiently thick organic bulk heterojunction solar cells. Whereas in thin cells close to the first interference maximum the effect is minor, in thicker cells around the second interference maxima the space charge has a larger effect on device performance. Already small doping concentrations in the range of $N_A = 10^{16}$ cm^{-3} lead to the creation of a field-free

dx.doi.org/10.1021/jz301639y | J. Phys. Chem. Lett. 2012, 3, 3470–3475

region with low carrier collection efficiency. Optimizing the device performance of thick cells (d > 100 nm) means to maximize the overlap between the position dependent charge carrier collection efficiency and the optical generation rate.

EXPERIMENTAL DETAILS

Materials. Si-PCPDTBT was supplied by Konarka Technologies. $PC_{70}BM$ was supplied by Solenne BV. All of these materials were used as received. Solutions: Si-PCPDTBT:$PC_{70}BM$ (67 wt % $PC_{70}BM$, total concentration 40 mg/mL) solutions were prepared using orthodichlorobenzene. The solution was stirred overnight to promote complete dissolution. Devices: Bulk-heterojunction solar cells with the sandwich structure glass/ITO/PEDOT:PSS ∼(30 nm)/Si-PCPDTBT:PC70BM(1:2)/Ca(20 nm)/Al (100 nm) were fabricated by spin coating. Different thicknesses were obtained by varying the spinning speed from 500 to 2750 rpm. Thicknesses were measured with an Alphastep profilometer.

JV Measurements. Device efficiencies and *JV* characteristics were measured by using Keithley 238 Source Measure Units. Illumination was provided using a 300W xenon arc lamp solar simulator (Oriel Instruments) and calibrated using a silicon photodiode to ensure the illumination intensity of 100 mW/cm^2. During the measurements, the devices were kept in a nitrogen environment in a sealed chamber

Ellipsometry. Variable angle spectroscopic ellipsometry data were recorded using a rotating polarizer GES5E ellipsometer with CCD detection from SOPRALAB for films of different compositions deposited on quartz and on silicon. The complex refractive indices for the thin films were modeled by fitting the experimental data using the standard critical point model of the dielectric function.[46] We note that the addition of anisotropy in the model did not improve the quality of the fit, and, moreover, modeling of the blend films by the effective medium approximation (Bruggeman) of the pure materials did not result in good fits of the experimental data.

ASSOCIATED CONTENT

Supporting Information

Capacitance/voltage measurements used for the determination of doping concentrations. Complex refractive index of the active layer as determined from ellipsometry. Chemical structure of the polymer and schematic of the layer stack as well as position-dependent generation rates, a detailed list of parameters for the simulations, and simulations on p-type and n-type doping with variable doping concentrations. Discussion of the effects of field-dependent charge generation and of spatially inhomogeneous doping on the current/voltage curves. Discussion of the charge carrier concentration dependence of the mobility-lifetime product. This material is available free of charge via the Internet at http://pubs.acs.org.

AUTHOR INFORMATION

Notes

The authors declare no competing financial interest.

ACKNOWLEDGMENTS

We thank Pabitra Shakya Tuladhar for help with sample preparation. W.G. acknowledges support from P.R. China's State Scholarship Fund. T.K. acknowledges support by an Imperial College Junior Research Fellowship.

REFERENCES

(1) Street, R. A.; Schoendorf, M.; Roy, A.; Lee, J. H. Interface State Recombination in Organic Solar Cells. *Phys. Rev. B* **2010**, *81*, 205307.
(2) Tumbleston, J. R.; Liu, Y. C.; Samulski, E. T.; Lopez, R. Interplay Between Bimolecular Recombination and Carrier Transport Distances in Bulk Heterojunction Organic Solar Cells. *Adv. Energy Mater.* **2012**, *2*, 477−486.
(3) Street, R. A.; Krakaris, A.; Cowan, S. R. Recombination Through Different Types of Localized States in Organic Solar Cells. *Adv. Funct. Mater.* **2012**, *22*, 4608−4619.
(4) Peet, J.; et al. Bulk Heterojunction Solar Cells With Thick Active Layers and High Fill Factors Enabled by a Bithiophene-Co-Thiazolothiazole Push-Pull Copolymer. *Appl. Phys. Lett.* **2011**, *98*, 043301.
(5) Hoppe, H.; Shokhovets, S.; Gobsch, G. Inverse Relation Between Photocurrent and Absorption Layer Thickness in Polymer Solar Cells. *Phys. Status Solidi RRL* **2007**, *1*, R40−R42.
(6) Dennler, G.; Scharber, M. C.; Brabec, C. J. Polymer-Fullerene Bulk-Heterojunction Solar Cells. *Adv. Mater.* **2009**, *21*, 1323−1338.
(7) Credgington, D.; Hamilton, R.; Atienzar, P.; Nelson, J.; Durrant, J. R. Non-Geminate Recombination As the Primary Determinant of Open-Circuit Voltage in Polythiophene:Fullerene Blend Solar Cells: an Analysis of the Influence of Device Processing Conditions. *Adv. Funct. Mater.* **2011**, *21*, 2744−2753.
(8) Lee, S.; Nam, S.; Kim, H.; Kim, Y. Organic Solar Cells With Submicron-Thick Polymer:Fullerene Bulk Heterojunction Films. *Appl. Phys. Lett.* **2010**, *97*, 103503.
(9) Zeng, L. C.; Tang, C. W.; Chen, S. H. Effects of Active Layer Thickness and Thermal Annealing on Polythiophene: Fullerene Bulk Heterojunction Photovoltaic Devices. *Appl. Phys. Lett.* **2010**, *97*, 053305.
(10) Price, S. C.; Stuart, A. C.; Yang, L. Q.; Zhou, H. X.; You, W. Fluorine Substituted Conjugated Polymer of Medium Band Gap Yields 7% Efficiency in Polymer-Fullerene Solar Cells. *J. Am. Chem. Soc.* **2011**, *133*, 4625−4631.
(11) Hoppe, H.; Arnold, N.; Sariciftci, N. S.; Meissner, D. Modeling the Optical Absorption Within Conjugated Polymer/Fullerene-Based Bulk-Heterojunction Organic Solar Cells. *Sol. Energy Mater. Sol. Cells* **2003**, *80*, 105−113.
(12) Andersson, B. V.; Huang, D. M.; Moule, A. J.; Inganas, O. An Optical Spacer Is No Panacea for Light Collection in Organic Solar Cells. *Appl. Phys. Lett.* **2009**, *94*, 043302.
(13) Kotlarski, J. D.; Blom, P. W. M.; Koster, L. J. A.; Lenes, M.; Slooff, L. H. Combined Optical and Electrical Modeling of Polymer: Fullerene Bulk Heterojunction Solar Cells. *J. Appl. Phys.* **2008**, *103*, 084502.
(14) Lenes, M.; Koster, L. J. A.; Mihailetchi, V. D.; Blom, P. W. M. Thickness Dependence of the Efficiency of Polymer: Fullerene Bulk Heterojunction Solar Cells. *Appl. Phys. Lett.* **2006**, *88*, 243502.
(15) Soldera, M.; Taretto, K.; Kirchartz, T. Comparison of Device Models for Organic Solar Cells: Band-to-Band Vs. Tail States Recombination. *Phys. Status Solidi A* **2012**, *209*, 207−215.
(16) Street, R. A.; Cowan, S.; Heeger, A. J. Experimental Test for Geminate Recombination Applied to Organic Solar Cells. *Phys. Rev. B* **2010**, *82*, 121301.
(17) Shuttle, C. G.; Hamilton, R.; O'Regan, B. C.; Nelson, J.; Durrant, J. R. Charge-Density-Based Analysis of the Current-Voltage Response of Polythiophene/Fullerene Photovoltaic Devices. *Proc. Natl. Acad. Sci. U.S.A.* **2010**, *107*, 16448−16452.
(18) Jamieson, F. C.; Agostinelli, T.; Azimi, H.; Nelson, J.; Durrant, J. R. Field-Independent Charge Photogeneration in PCPDTBT/PC70BM Solar Cells. *J. Phys. Chem. Lett.* **2010**, *1*, 3306−3310.
(19) Maurano, A.; et al. Recombination Dynamics As a Key Determinant of Open Circuit Voltage in Organic Bulk Heterojunction Solar Cells: A Comparison of Four Different Donor Polymers. *Adv. Mater.* **2010**, *22*, 4987−4992.
(20) Crandall, R. S. Transport in Hydrogenated Amorphous-Silicon P-I-N Solar-Cells. *J. Appl. Phys.* **1982**, *53*, 3350−3352.

(21) Bisquert, J.; Garcia-Belmonte, G. On Voltage, Photovoltage, and Photocurrent in Bulk Heterojunction Organic Solar Cells. *J. Phys. Chem. Lett.* **2011**, *2*, 1950−1964.
(22) Kirchartz, T.; Nelson, J. Meaning of Reaction Orders in Polymer:Fullerene Solar Cells. *Phys. Rev. B* **2012**, *86*, 165201.
(23) Mihailetchi, V. D.; Wildeman, J.; Blom, P. W. M. Space-Charge Limited Photocurrent. *Phys. Rev. Lett.* **2005**, *94*, 126602.
(24) Azimi, H.; Senes, A.; Scharber, M. C.; Hingerl, K.; Brabec, C. J. Charge Transport and Recombination in Low-Bandgap Bulk Heterojunction Solar Cell Using Bis-Adduct Fullerene. *Adv. Energy Mater.* **2011**, *1*, 1162−1168.
(25) Morana, M.; et al. Nanomorphology and Charge Generation in Bulk Heterojunctions Based on Low-Bandgap Dithiophene Polymers With Different Bridging Atoms. *Adv. Funct. Mater.* **2010**, *20*, 1180−1188.
(26) Scharber, M. C.; et al. Influence of the Bridging Atom on the Performance of a Low-Bandgap Bulk Heterojunction Solar Cell. *Adv. Mater.* **2010**, *22*, 367−370.
(27) Kotlarski, J. D.; Blom, P. W. M. Impact of Unbalanced Charge Transport on the Efficiency of Normal and Inverted Solar Cells. *Appl. Phys. Lett.* **2012**, *100*, 013306.
(28) Kotlarski, J. D.; Moet, D. J. D.; Blom, P. W. M. Role of Balanced Charge Carrier Transport in Low Band Gap Polymer:Fullerene Bulk Heterojunction Solar Cells. *J. Polym. Sci., Part B: Polym. Phys.* **2011**, *49*, 708−711.
(29) Glatthaar, M.; Riede, M.; Keegan, N.; Sylvester-Hvid, K.; Zimmermann, B.; Niggemann, M.; Hinsch, A.; Gombert, A. Efficiency Limiting Factors of Organic Bulk Heterojunction Solar Cells Identified by Electrical Impedance Spectroscopy. *Sol. Energy Mater. Sol. Cells* **2007**, *91*, 390−393.
(30) Fabregat-Santiago, F.; Garcia-Belmonte, G.; Mora-Sero, I.; Bisquert, J. Characterization of Nanostructured Hybrid and Organic Solar Cells by Impedance Spectroscopy. *Phys. Chem. Chem. Phys.* **2011**, *13*, 9083−9118.
(31) Kirchartz, T.; Gong, W.; Hawks, S. A.; Agostinelli, T.; MacKenzie, R. C. I.; Yang, Y.; Nelson, J. Sensitivity of the Mott-Schottky Analysis in Organic Solar Cells. *J. Phys. Chem. C* **2012**, *116*, 7672−7680.
(32) Trukhanov, V. A.; Bruevich, V. V.; Paraschuk, D. Y. Effect of Doping on Performance of Organic Solar Cells. *Phys. Rev. B* **2011**, *84*, 205318.
(33) Khelifi, S.; Decock, K.; Lauwaert, J.; Vrielinck, H.; Spoltore, D.; Piersimoni, F.; Manca, J.; Belghachi, A.; Burgelman, M. Investigation of Defects by Admittance Spectroscopy Measurements in Poly (3-Hexylthiophene):(6,6)-Phenyl C(61)-Butyric Acid Methyl Ester Organic Solar Cells Degraded Under Air Exposure. *J. Appl. Phys.* **2011**, *110*, 094509.
(34) Stelzl, F. F.; Wurfel, U. Modeling the Influence of Doping on the Performance of Bulk Heterojunction Organic Solar Cells: One-Dimensional Effective Semiconductor Versus Two-Dimensional Donor/Acceptor Model. *Phys. Rev. B* **2012**, *86*, 075315.
(35) Heath, J.; Zabierowski, P. Capacitance Spectroscopy of Thin-Film Solar Cells. In *Advanced Characterization Techniques for Thin Film Solar Cells*; Abou-Ras, D., Kirchartz, T., Rau, U., Eds.; Wiley-VCH: Weinheim, Germany, 2011; pp 81−105.
(36) Liang, Z. Q.; Gregg, B. A. Compensating Poly(3-Hexylthiophene) Reveals Its Doping Density and Its Strong Exciton Quenching by Free Carriers. *Adv. Mater.* **2012**, *24*, 3258−3262.
(37) Abdou, M. S. A.; Orfino, F. P.; Son, Y.; Holdcroft, S. Interaction of Oxygen With Conjugated Polymers: Charge Transfer Complex Formation With Poly(3-Alkylthiophenes). *J. Am. Chem. Soc.* **1997**, *119*, 4518−4524.
(38) Boix, P. P.; Garcia-Belmonte, G.; Munecas, U.; Neophytou, M.; Waldauf, C.; Pacios, R. Determination of Gap Defect States in Organic Bulk Heterojunction Solar Cells From Capacitance Measurements. *Appl. Phys. Lett.* **2009**, *95*, 233302.
(39) Kirchartz, T.; Pieters, B. E.; Kirkpatrick, J.; Rau, U.; Nelson, J. Recombination Via Tail States in Polythiophene: Fullerene Solar Cells. *Phys. Rev. B* **2011**, *83*, 115209.
(40) Slooff, L. H.; Veenstra, S. C.; Kroon, J. M.; Moet, D. J. D.; Sweelssen, J.; Koetse, M. M. Determining the Internal Quantum Efficiency of Highly Efficient Polymer Solar Cells Through Optical Modeling. *Appl. Phys. Lett.* **2007**, *90*, 143506.
(41) Burkhard, G. F.; Hoke, E. T.; McGehee, M. D. http://www.stanford.edu/group/mcgehee/transfermatrix/, 2010 (accessed August 3, 2012).
(42) Burkhard, G. F.; Hoke, E. T.; McGehee, M. D. Accounting for Interference, Scattering, and Electrode Absorption to Make Accurate Internal Quantum Efficiency Measurements in Organic and Other Thin Solar Cells. *Adv. Mater.* **2010**, *22*, 3293−3297.
(43) Pettersson, L. A. A.; Roman, L. S.; Inganas, O. Modeling Photocurrent Action Spectra of Photovoltaic Devices Based on Organic Thin Films. *J. Appl. Phys.* **1999**, *86*, 487−496.
(44) Sievers, D. W.; Shrotriya, V.; Yang, Y. Modeling Optical Effects and Thickness Dependent Current in Polymer Bulk-Heterojunction Solar Cells. *J. Appl. Phys.* **2006**, *100*, 114509.
(45) Hecht, Z. Zum Mechanismus Des Lichtelektrischen Primärstromes in Isolierenden Kristallen. *Z. Phys. A* **1932**, *77*, 235−245.
(46) Campoy-Quiles, M.; Nelson, J.; Bradley, D. D. C.; Etchegoin, P. G. Dimensionality of Electronic Excitations in Organic Semiconductors: A Dielectric Function Approach. *Phys. Rev. B* **2007**, *76*, 235206.